Relation between shape and the phenomenon of flutter for bridge deck-like bluff bodies

T. NOWICKI[1], A. FLAGA[2]

[1] *Department of Structural Mechanics*
Faculty of Civil Engineering and Architecture
Lublin University of Technology
Nadbystrzycka 40
20-618 Lublin, Poland
e-mail: t.nowicki@pollub.pl

[2] *Wind Engineering Laboratory*
Institute of Structural Mechanics
Cracow University of Technology
Al. Jana Pawła II 37/3a
31-864 Kraków, Poland
e-mail: liwpk@windlab.pl

THE PAPER DEALS WITH experimental analysis of the influence of cross–section shape of a body on the phenomenon of flutter. The aeroelastic section model that was the object of study in a laboratory corresponded to a central section of a long bridge deck. Such structures are subjected to flutter like aeroplane wings or helicopter rotors. Unlike in aviation, bridge decks cross-sections can be designed much more freely. The analysis is concentrated on a problem how the cross-section shape of a deck can affect interaction with incoming air stream. The results obtained suggest that the influence is closely related to elastic characteristics of a deck.[*]

Key words: structure-fluid interaction, flutter, cable–stayed bridges, suspension bridges.

Notations

L length, m,
B width, m,
m mass, kg,
I moment of inertia, $\text{kg} \cdot \text{m}^2$,
f_1 frequency of vertical vibration, Hz,
f_2 frequency of rotational vibration, Hz,
f_3 dominant frequency of flutter, Hz,

V_1 flutter onset velocity, m/s,
V_2 flutter fading velocity, m/s,
V_3 flutter disappearance velocity, m/s.

1. Motivation

The research on flutter in civil engineering has been carried out since the collapse of the Tacoma Narrows Bridge (USA) in 1940. The catastrophe was a direct result of flutter that developed on the bridge deck at wind speed of 18.8 m/s. The velocity did not exceed the value for which the structure was designed. The reason was that the project was done without taking into consideration possible interaction between the bridge deck and incoming air stream. Although the phenomenon of flutter was known in aviation, it was still neglected in civil engineering those days. Even excessive oscillation of the structure during assembly work did not raise any alarm strong enough to reconsider the design. It was only the collapse that initiated an interest in fluid interaction with solids in the field of big buildings. Nowadays, the risk of developing aeroelastic instabilities is always the matter while designing any lightweight longspan structures. In the case of cable-stayed bridges it is most important to prove that a deck or a part of it (usually central) is incapable of developing flutter at wind speeds that are expected.

Modern design engineer's workshop includes CFD tools, aerodynamic wind tunnels and many simple empirical and semi-empirical models of flutter [1]. The most reliable results come, of course, from wind tunnel tests and computer simulations. However, simpler methods connected with engineering experience and intuition are invaluable because they indicate initial solutions and make possible further work. Common disadvantage of the simple models is their close connection with cross-section shape of a deck, i.e. they are valid for the shapes for which they were derived. The fact limits their scope of application.

Since last decades many in-depth analyses in the field of flutter have been preformed. Research work has applied a wide range of wind engineering methods developed after the collapse of Tacoma [2]. Although researchers agree that the cross-section shape of a bridge deck is one of the most important factors in aerodynamic response of a structure in air stream, the problem itself has not been treated widely so far. Papers are usually devoted to development or verification of theoretical methods and assume specific cross-section shapes and its suspension parameters, often corresponding to real structures. The problem of shape is solved by introducing empirical coefficients that must be estimated in wind tunnel tests [3–5] or do not occur due to quality of a method [6–8]. Conclusions about influence of cross-section shape can be found in literature [9], but not as a key question.

The main motivation of research presented in this paper was to find out how the shape of a solid immersed in fluid influences the interaction between them.

The intention of direct application to building structure mechanics explains the choice of methodology and the object of the research. Presented results result only from experimental work, which is their undoubted value. They can be therefore used as a verification test for any theoretical methods, models and formulae.

2. Wind tunnel

The experiment was preformed in Wind Engineering Laboratory of the Cracow University of Technology. The laboratory contains a boundary layer wind tunnel with a working section of internal dimensions 2.2 m width, 1.6 m height and 10 m length. In order to minimize the blockage effect, its both side-walls are constructed as slotted walls with horizontal adjustable gaps. The floor and ceiling are solid and let adjust height of the section. The maximum flow speed is 40 m/s. There are possible 2 circuit modes of the air flow: closed and opened. All of the presented tests in this paper were carried out in the closed mode circuit.

3. Model and measurement set-up

The object of the study was an aeroelastic system placed in an air stream (Fig. 1). The system was designed to satisfy the criteria of similarity to a central section of a cable stayed bridge deck (Fig. 2). However, the model did not imitate any existing structure because such buildings are not (or should not be) prone to flutter, while the aim of the experiment was to induce such phenomena and to examine them.
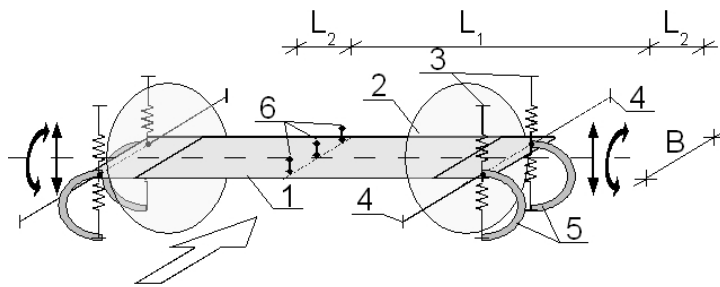

Fig. 1. Schematic view of the model: 1 – carrying plate, 2 – end plates, 3 – springs, 4 – strings, 5 – dampers, 6 – accelerometers; $L_1 = 2.12$ m, $L_2 = 0.14$ m, $B = 0.4$ m; arrows show the degrees of freedom.

The model was symmetrical. A carrying base was a plate 2.4 m long, 0.4 m wide and 0.018 m thick, made of a composite plate *ESACORE–ST*, produced by Italian company *Metalleid Componets*. The plate was a sandwich panel based on honeycomb technology, with an aluminium core and double-sided skin in HPL laminate. High stiffness at low mass characterise the panel. Round plates 0.4 m
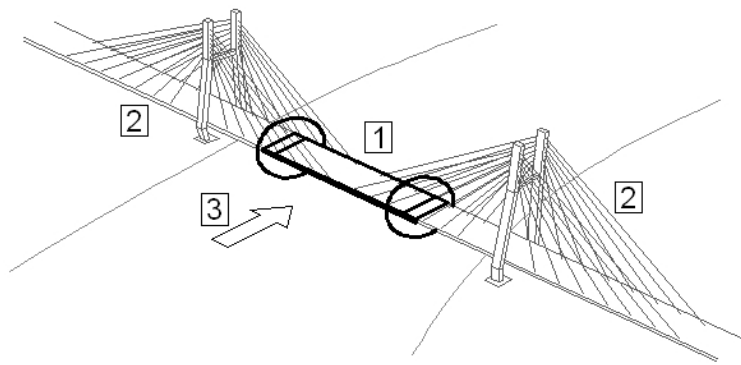
Fig. 2. Schematic view of a cable stayed bridge: 1 – central part that was modelled,
2 – outer parts incapable of flutter replaced with suspension, 3 – air stream.

in diameter made of transparent organic glass were fixed at both ends of the plate, 0.14 m from its edges. The end plates main task was to reduce the flow disturbance at both ends of the model. The central part between the end plates subjected to air stream was 2.12 m long. The model ends were placed outside the working section of the wind tunnel and had adjustable handles for springs, strings and rubber belts. The ends were extra strengthened in case of loosing control of the model during tests, which could lead to coming up from the suspension and hitting other parts of the tunnel. Three sockets for accelerometers were stuck in the symmetry axis of the model. All other connections were made of aluminium shapes and steel screws. After assembling the model, frequency of free vibration of the carrying plate was measured. The result was 6.9Hz for the first mode obtained for both ends single-supported at lines of the hangers.

Suspension consisted of vertical steel springs, horizontal strings and optional rubber belts. Eight steel springs of 360 N/m linear stiffness were used – two pairs at each model end. One pair consisted of 2 springs mounted on opposite sides of the board in a handle. The other ends of the springs were fixed to a steel frame which was equipment of the wind tunnel. Movable arms of the frame let tension the system of springs. The springs could be mounted symmetrically with respect to the model axis of rotation in 6 spaces: 0.18, 0.22, 0.26, 0.30, 0.38 m. The task of the horizontal strings was to constrain the model horizontal degree of freedom with small interference of other degrees. The strings were 1.3 m long and were fixed to the springs hangers. The other ends of them were mounted to stable elements of tunnel walls. Two pairs of rubber belts mounted at each end in the springs hangers were optional supplement of the suspension. The main task of them was to increase the damping parameters. The belts connected the model with the tunnel frame in this way that they shaped a letter 'C' under the model. Such configuration let them damp the motion of the model with little change in

stiffness of the suspension. The belts were made of 2 layers of rubber connected with double-sided adhesive tape, which increased their ability to dissipate energy.

The cross-section of the model was modified by adding to the main board the prismatic blocks made of hard foamed polystyrene EPS–100 (Fig. 3). All the cross-sections were symmetrical and corresponded to real shapes of bridge decks. Finally, the four different cross-sections were examined: rectangular base plate and 3 modifications.
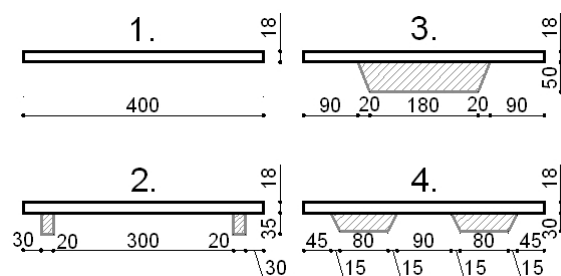

Fig. 3. Cross-section under interest: 1 – base model, 2, 3, 4 – modifications (dimensions in mm).

The model was placed crosswise in the working section of the wind tunnel (Fig. 4), 0.55 m above the tunnel floor, so the distance to the ceiling was 1.05 m. Turbulence intensity at the level was 5%. The ends of the model and all elements of the suspension were placed outside the working section and were covered by the end plates. Acceleration of the model was measured at the central line of the model, which coincided with a symmetry plane of the tunnel, with 3 uniaxial accelerometers *HBN B12/200*, A/C converter *Spider 8* and a computer program *Catman* running on a PC computer. One accelerometer was placed at the axis of
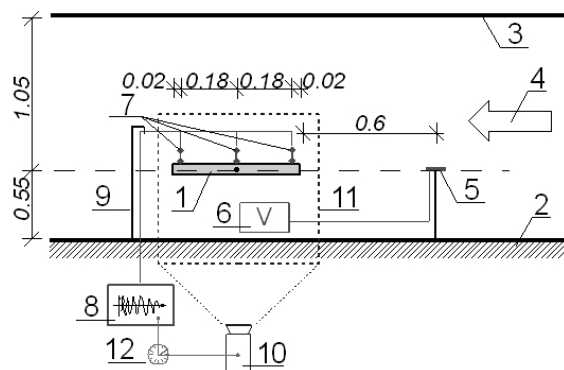

Fig. 4. Diagram of measurement set-up: 1 – model, 2 – wind tunnel working section floor, 3 – ceiling, 4 – turn of the air flow, 5, 6 – electronic anemometer with a display, 7, 8 – accelerometers with an A/D converter and a computer, 9 – cable support, 10 – digital camera, 11 – recordedframe, 12 – time synchronization (dimensions in m).

rotation and others at the distance of 0.02 m from edges of the main board. Mass of each accelerometer was 0.025 kg. Their cables were installed on the leeward side and supported. Measured signal was recorded on a hard disc drive.

Velocity of the air stream was measured with an electronic anemometer, the sensor being placed on the symmetry plane of the tunnel, at the level of the model i.e. 0.6 m in front of it. The anemometer had a big electronic display easy to film. It was mounted outside the working section next to the model. Aerodynamic response of the model was recorded with a digital camera. The frame included an end elevation view of the model and the display. At every turn, time synchronization between the PC computer and the camera was done.

4. Parameters of the model

The aeroalastic system was symmetrical and was symmetrically placed in the tunnel. The symmetry applied to its geometry, mass distribution, suspension characteristics and the air flow. The carrying plate, in comparison with stiffness of the suspension, could be considered as rigid. The proportion of working part of the model was $L_1/B > 5$. The end plates with cooperation with the tunnel slotted walls minimize the flow disturbance at the ends of the model. The strings constrained horizontal degree of freedom with small effect on other directions. For this reason, the system can be reduced in analysis to a 2D case (Fig. 5).
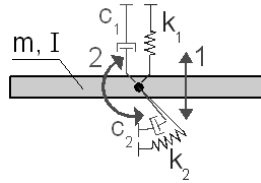

Fig. 5. 2D simplification of the aeroelastic system: 1 – vertical degree of freedom, 2 – rotational degree of freedom, m – mass, I – moment of inertia, k_1, k_2 – stiffness parameters, c_1, c_2 – damping parameters.

The simplified system has 2 degrees of freedom: 1) vertical motion and 2) rotation. Such system can be defined by its inertia characteristics: mass m and moment I, resultant stiffness k_1, k_2 and damping c_1, c_2 and finally – its geometry. If x denotes the vertical displacement and α the rotation, the equations of motion are:

(4.1)
$$m\ddot{x} + c_1\dot{x} + k_1 x = P,$$
$$I\ddot{\alpha} + c_2\dot{\alpha} + k_2\alpha = M,$$

where resultant force P and moment M must be strongly dependent on deck geometry, because both follow the pressure dynamically distributed on external surface of a body.

The model at each modification was weighed. Moments of inertia were calculated on the basis of known geometry and mass of the component parts. In order to find stiffness and damping parameters, the system was put into oscillations by displacing it from the state of equilibrium and releasing. Independent tests were preformed for vertical and rotational degrees of freedom. Analysis of the recorded acceleration and determined earlier inertia parameters enables to determine the missing characteristic.

The following tables present resultant parameters of the model. Table 1 shows inertia parameters of the model for each version. As one can see, the modifications did not increase the model mass more then 6%. Changes in the moment of inertia were smaller and did not exceed 2%.

Table 1. Inertia parameters of the system.

Section	Mass		Moment of inertia	
	[kg]	[%]	$[\mathrm{kg} \cdot \mathrm{m}^2]$	[%]
1	7.44	100.0	0.1983	100.0
2	7.50	100.8	0.1998	100.8
3	7.87	105.7	0.2003	101.0
4	7.69	103.2	0.2010	101.4

Table 2 presents stiffness characteristics of the model suspension. The parameters were determined on the assumption that for the system without C dampers installed the frequency of decaying oscillations equals the frequency of free vibration. The rotational stiffness increased with extending distance between the springs, while the vertical stiffness remained untouched.

Table 2. Stiffness parameters of the system.

Spring spacing [m]	Vertical stiffness k_1 [N/m]	Rotational stiffness k_2 [$\mathrm{N} \cdot \mathrm{m/rad}$]
0.18		48.6
0.22		59.6
0.26	2610	73.1
0.30		87.7
0.34		107
0.38		128

Table 3 gives damping parameters of the system for its degrees of freedom. The values are mean and come from decaying oscillations tests for every configuration of the system. As one can see, the levels of damping differed significantly.

Table 3. Damping parameters of the system.

Level	Vertical damping c_1		Rotational damping c_2	
	[kg/s]	[%]	[kg·m^2/s]	[%]
–	1.21	100	0.0273	100
C dampers	2.66	220	0.0833	306

All the modifications in the cross-section shape did not result in significant changes in inertia characteristics and, of course, did not change the suspension. Rubber C dumpers did not influence the system stiffness and mass noticeably, yet the change was taken into consideration (explained later). To sum up, the aeroelastic system was examined in 4 different cross-section shapes for 6 values of rotational stiffness (at the same value of vertical stiffness) and at 2 levels of damping. All the tests were preformed at air temperature of 20–22°C.

5. Procedure of experiment

For each cross-section shape the same procedure was performed. The springs were set in each of 6 distances in turn. First the model was displaced from its point of balance in order to determine its characteristics as it was mentioned previously, next three tests in air stream were made. Then the suspension were supplemented with the C dampers and the procedure was repeated. Finally, $4 \times 6 \times 2 = 48$ different configurations were tested. Flutter occurred in 43 configurations as self-induced phenomena. No additional external excitation was applied. In spite of great care, in 3 cases the phenomenon developed too rapidly making the model impossible to control, which led to coming the model up the suspension. A typical course of a flutter test is presented in Fig. 6.

The velocity of the air flow was increased until flutter occurred due to self-contained excitation. Then it was held approximately constant until oscillations of the model exceeded safe levels. Next, the velocity was reduced implicating fading of the phenomena. Three characteristic points were distinguished. The phenomena started at point 1 (see Fig. 6) when amplitudes of measured accelerations began to grow. At point 2 the accelerations began to decrease, what means that the flutter faded until it disappeared at point 3. Stream velocities corresponding to the points were named: flutter onset V_1, flutter fading V_2 and flutter disappearance V_3, respectively. The first two velocities are strictly connected with the aeroelastic behaviour of the system. The last one describes the system ability to dump its oscillations in the presence of vanishing flow. All of them are of structural analysts' interest. Another flutter characteristic, which was under investigation, was its frequency. The phenomenon each time developed one dominant frequency (see Fig. 7). It was always the first one.
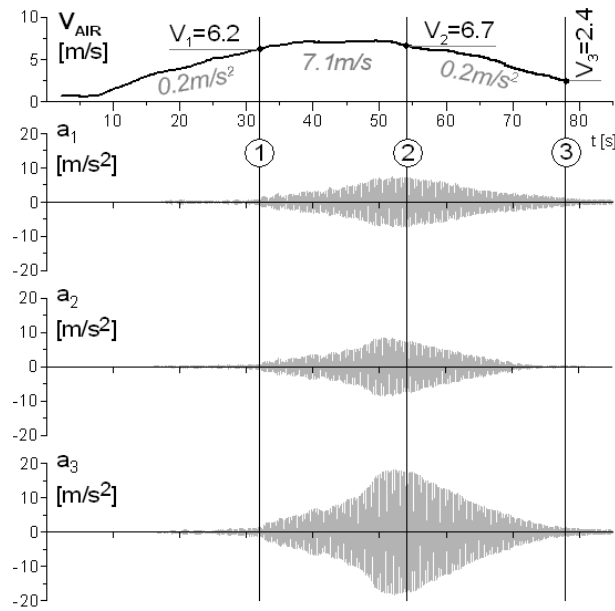
FIG. 6. Course of flutter test for cross-section 3, spring distance 0.34 m without C dumpers. Accelerometers numbered in accordance with the incoming flow. See also Fig. 1 and 4.
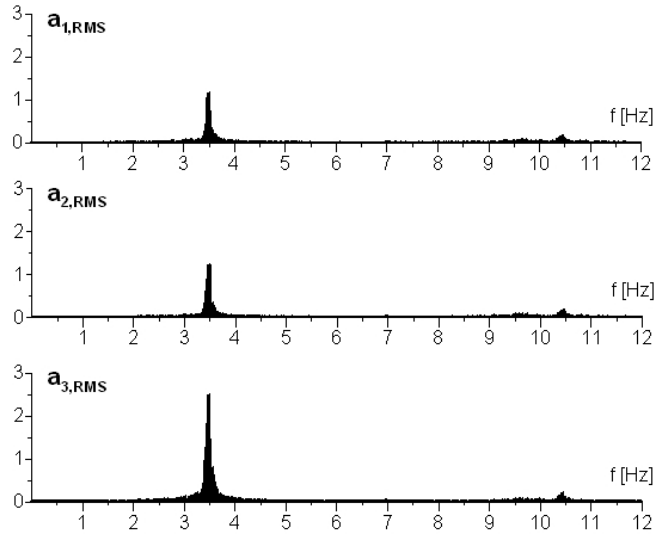

FIG. 7. Frequency analysis of the signal presented in Fig. 6.

During each course of flutter, the amplitudes and frequencies of acceleration measured in 3 points changed in time. A typical change in amplitude for a system without the C dumpers is presented in Fig. 6. The amplitude increased due to

positive feedback of aerodynamic forces and decreased after reducing the speed of the air flow. It had a tendency to increase at a constant air stream speed level, which run the risk of breaking the model. After connecting the C dampers the amplitude did not grow so rapidly as before. In same configuration of the system it was possible to keep it at an approximately constant level for unchanging air stream velocity, albeit it was still possible to distinguish the 3 characteristic points of a flutter course and determine the velocities under interest. The change in frequency cannot be noticed in Fig. 6 because the diagram covers too long range of time. Figure 8 shows the measured frequency as a function of time. The differences in the values was reduced while flutter developed heading for a specific value, which can be determined with an acceptable accuracy by modal analysis of the signal (see Fig. 7). Changes in frequency values in the last stage of the course were the result of the fading phenomena.
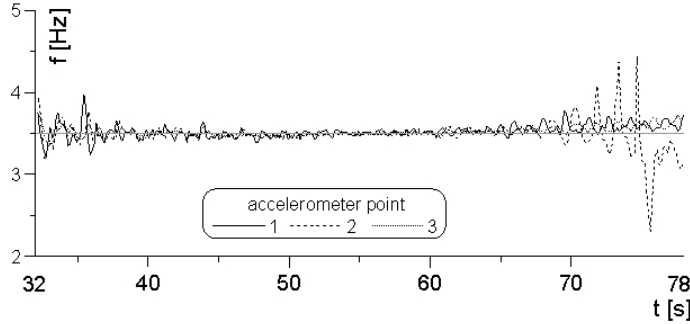

Fig. 8. Change in frequency during the test presented in Fig. 6.

6. Results and discussion

The following tables and diagrams show the obtained results: air stream velocities for flutter: onset V_1, fading V_2 and disappearing V_3 as well as the dominant flutter frequency f_3. The values have been correlated with frequencies of decaying oscillations of the system. The frequencies: f_1 – for vertical degree of freedom and f_2 – for the rotational one, were determined for every assembled configuration of the model. For this reason, the frequency ratio f_2/f_1 was recognized as the best parameter describing the suspension. The values depended mainly on the springs settings but as the resultant ones, they took into account effects of the C dampers and changes in inertia characteristics. The frequency f_1 was chosen as a basis because it changed the least.

Tables from 4 to 7 give the measured values of Sect. 1 to 4 respectively for the 6 different distance settings between the springs. The first parts of the tables present results for the system without the C dampers, while the second parts – with the C dampers installed. The given values are average for 3 independent

tests. Additionally observed form of flutter has been enclosed. The first symbol indicates the dominant form: R – rotational, V – vertical. The second symbol says which edge of the model oscillated with larger amplitude: W – windward, L – leeward. The symbol 0 means that any dominance could not be observed in both cases. The last columns of the tables contain values of the kinematic flutter Strouhal numbers calculated for each case, taking into consideration the onset

Table 4. Cross-section 1.

Set	f_1	f_2	f_2/f_1	f_3	f_3/f_1	V_1	V_2	V_3	Form	St
[m]	[Hz]	[Hz]	[–]	[Hz]	[–]	[m/s]	[m/s]	[m/s]		[–]
0.18	2.97	2.42	0.81	×	×	×	×	×	×	×
0.22	2.97	2.73	0.92	×	×	×	×	×	×	×
0.26	2.97	3.04	1.02	×	×	13.9	×	×	V, 0	×
0.30	2.97	3.37	1.14	3.24	1.09	7.40	7.37	4.82	0, L	0.18
0.34	2.97	3.74	1.26	3.50	1.18	7.24	7.56	6.11	R, L	0.19
0.38	2.97	3.96	1.33	3.69	1.25	8.39	8.12	5.87	R, L	0.18
0.18	2.88	2.59	0.90	×	×	×	×	×	×	×
0.22	2.88	2.85	0.99	×	×	×	×	×	×	×
0.26	2.88	3.11	1.08	×	×	×	×	×	×	×
0.30	2.89	3.37	1.16	3.18	1.10	7.64	8.20	5.75	0, L	0.17
0.34	2.89	3.70	1.28	3.50	1.21	8.44	8.24	6.87	R, L	0.17
0.38	2.86	3.88	1.36	3.69	1.29	8.31	8.71	6.70	R, L	0.18

(rows 7–12: C dampers)

Table 5. Cross-section 2.

Set	f_1	f_2	f_2/f_1	f_3	f_3/f_1	V_1	V_2	V_3	Form	St
[m]	[Hz]	[Hz]	[–]	[Hz]	[–]	[m/s]	[m/s]	[m/s]		[–]
0.18	2.97	2.53	0.85	2.35	0.79	6.22	7.05	3.75	R, W	0.15
0.22	2.97	2.82	0.95	2.60	0.88	8.15	9.33	7.58	V, 0	0.13
0.26	2.97	3.11	1.05	3.10	1.04	8.17	9.73	5.71	V, L	0.15
0.30	2.97	3.41	1.15	3.36	1.13	4.66	4.50	2.49	R, L	0.29
0.34	3.00	3.74	1.24	3.56	1.18	4.90	4.78	3.70	R, L	0.29
0.38	3.00	4.10	1.37	3.94	1.31	6.15	6.06	3.22	R, L	0.26
0.18	2.97	2.71	0.91	2.32	0.78	7.77	9.46	7.18	R, 0	0.12
0.22	2.93	2.93	1.00	2.56	0.87	8.92	9.76	9.14	V, 0	0.11
0.26	2.86	3.15	1.10	3.09	1.08	6.11	6.32	3.48	0, L	0.20
0.30	2.93	3.44	1.17	3.31	1.13	5.52	5.87	3.56	R, L	0.24
0.34	2.93	3.70	1.26	3.55	1.21	6.99	6.99	5.23	R, L	0.20
0.38	2.93	4.03	1.37	3.85	1.31	7.29	7.56	4.23	R, L	0.21

(rows 7–12: C dampers)

flutter velocity V_1, dominant frequency f_3 and the body width B (Eq. 6.1).

(6.1) $$\mathrm{St} = \frac{f_3 B}{V_1}, \qquad B = 0.4 \text{ m}.$$

For the cross-section 1, the flutter occurred for a subset of configurations only. For the spring settings 0.18, 0.22 and 0.26 m, the phenomenon did not develop

Table 6. Cross-section 3.

	Set	f_1	f_2	f_2/f_1	f_3	f_3/f_1	V_1	V_2	V_3	Form	St
	[m]	[Hz]	[Hz]	[–]	[Hz]	[–]	[m/s]	[m/s]	[m/s]		[–]
	0.18	2.93	2.56	0.87	2.28	0.78	5.99	8.76	4.98	0, W	0.15
	0.22	2.89	2.75	0.95	2.57	0.89	7.56	9.17	6.03	V, 0	0.14
	0.26	2.89	3.04	1.05	3.03	1.05	7.40	7.44	2.97	V, 0	0.16
	0.30	2.89	3.33	1.15	3.25	1.12	6.38	7.10	2.92	0, L	0.20
	0.34	2.89	3.63	1.25	3.49	1.21	6.08	6.54	2.68	R, L	0.23
	0.38	2.89	3.96	1.37	3.76	1.30	6.94	7.61	3.03	R, L	0.22
C dampers	0.18	2.93	2.64	0.90	2.40	0.82	6.99	9.51	5.95	0, W	0.14
	0.22	2.86	3.22	1.13	2.86	1.00	7.34	8.39	4.96	V, 0	0.16
	0.26	2.93	3.37	1.15	3.07	1.05	6.46	7.96	3.67	0, 0	0.19
	0.30	2.82	3.37	1.19	3.19	1.13	8.12	8.88	6.03	0, L	0.16
	0.34	2.82	3.63	1.29	3.50	1.24	6.73	7.85	3.43	R, L	0.21
	0.38	2.82	3.88	1.38	3.48	1.23	7.72	9.46	6.00	R, L	0.18

Table 7. Cross-section 4.

	Set	f_1	f_2	f_2/f_1	f_3	f_3/f_1	V_1	V_2	V_3	Form	St
	[m]	[Hz]	[Hz]	[–]	[Hz]	[–]	[m/s]	[m/s]	[m/s]		[–]
	0.18	2.93	2.42	0.82	1.75	0.60	9.43	10.59	8.17	0, W	0.07
	0.22	2.93	2.70	0.92	2.15	0.73	11.31	13.56	10.29	V, W	0.08
	0.26	2.93	2.98	1.02	3.03	1.03	12.70	12.50	7.56	V, 0	0.10
	0.30	2.93	3.22	1.10	3.18	1.08	7.29	6.43	3.27	0, L	0.17
	0.34	2.93	3.66	1.25	3.44	1.17	7.77	7.37	3.89	R, L	0.18
	0.38	2.97	4.10	1.38	3.82	1.29	8.55	8.31	5.82	R, L	0.18
C dampers	0.18	2.86	2.44	0.85	1.89	0.66	*	*	*	0, W	*
	0.22	2.83	2.64	0.93	2.28	0.80	12.33	13.53	9.97	V, W	0.07
	0.26	2.86	2.93	1.03	2.92	1.02	13.24	11.60	8.58	V, 0	0.09
	0.30	2.86	3.30	1.15	3.14	1.10	7.64	7.64	3.54	0, L	0.16
	0.34	2.86	3.60	1.26	3.36	1.18	8.55	8.20	5.95	R, L	0.16
	0.38	2.86	3.97	1.39	3.61	1.26	9.43	9.41	6.73	R, L	0.15

* data lost due to a camera accident

under the flow speed below 15 m/s. The velocity was not increased further due to the risk of braking the model. For the setting 0.26 m with no optional dampers, the model preformed repeated vertical jumps. Such behaviour did not occur again.

For the cross-section 2, flutter occurred for every configuration of the system. For the lowest value of f_2/f_1, the movement of the model was rotational. As the ratio f_2/f_1 increased, the form became vertical and changed into rotational again for the next values. A similar change in the dominating edge of the moving model was noticed. At lower values of f_2/f_1 it was the windward edge of the model that performed larger oscillations. For a value close to 1.0 any domination could be noticed. At higher values of f_2/f_1, the leeward edge dominated.

For the cross-sections 3 and 4 flutter occurred for every configuration. The same change in flutter form was observed. The cross-section 1 followed the same pattern in the cases at which the flutter had developed. The vertical jumps suggested that the model could develop vertical mode flutter if the air stream velocity had been higher. In view of this it can be concluded that the transition in flutter form appeared for each cross-section shape with the change of the f_2/f_1 ratio. Significant change in damping parameters did not distort the behaviour.

The cross-section shape undoubtedly influenced the flutter characteristic velocities. The effect is depicted clearly in Fig. 9 to 14. It is easy to notice that 2
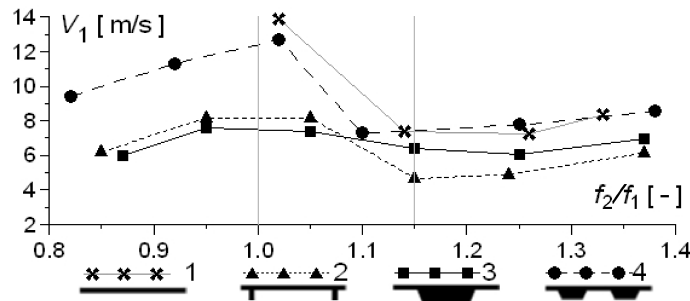

FIG. 9. Flutter onset velocity for the system without the C dampers.
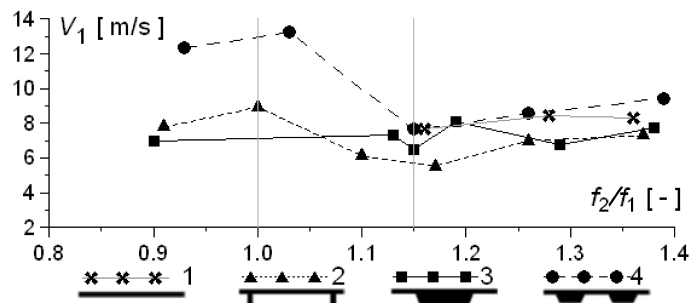

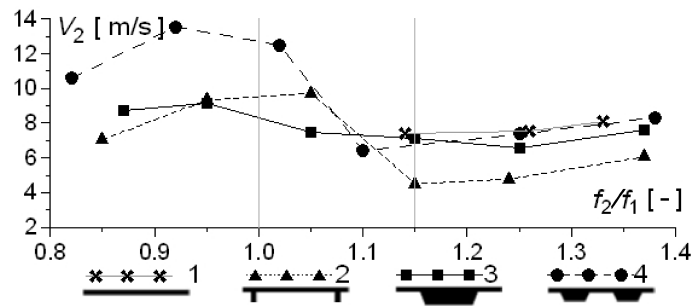FIG. 10. Flutter onset velocity for the system with the C dampers.

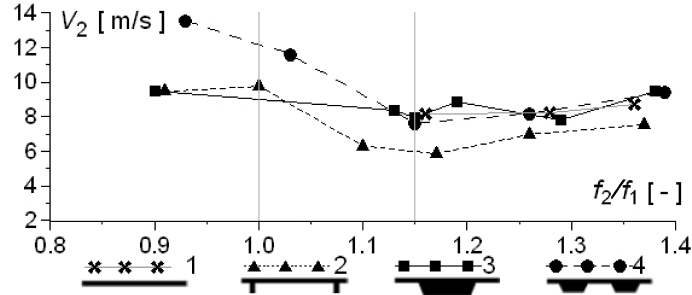Fig. 11. Flutter fading velocity for the system without the C dampers.

Fig. 12. Flutter fading velocity for the system with the C dampers.
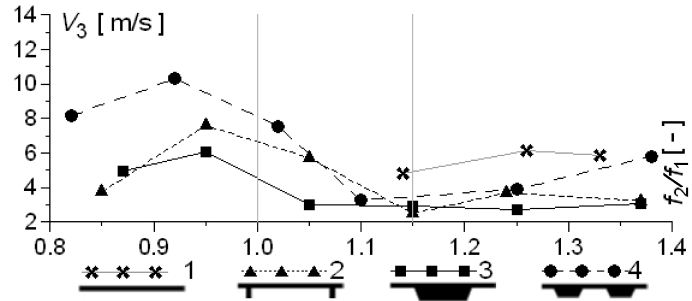

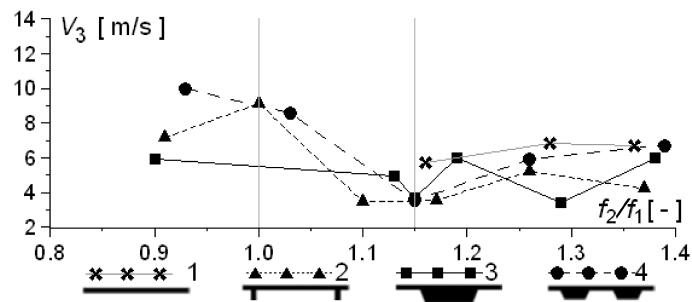Fig. 13. Flutter disappearance velocity for the system without the C dampers.

Fig. 14. Flutter disappearance velocity for the system with the C dampers.

different regions existed. For $f_2/f_1 < 1.15$, the shape played an important role in the fluid-structure interaction. For the ratio $f_2/f_1 > 1.15$ the shape lost its significance, i.e. the differences were smaller. For all model variants, the velocities attained their minima at the border of the regions, i.e. $f_2/f_1 = 1.15$. Within the first region it is easy to notice local maxima at the value of $f_2/f_1 \approx 1.0$, which may be surprising. Again the above observations involved all the cross-section shapes and were valid for the 2 different levels of damping.

The regions in the f_2/f_1 space were strictly correlated with the form of flutter. The first region was connected with the vertical form and domination of the windward edge, while the second one with rotational form and domination of the leeward edge. Gradual transition in the form took place within the interval $1.0 < f_2/f_1 < 1.15$.

The results obtained suggest that it may be difficult to predict aerodynamic response of a bridge deck after modification of its shape. Despite recognizable differences between the shapes 1 and 4, their characteristic flutter velocities were similar within the second region. Small modification to the base shape – compare the sections 1 and 2 – resulted in big change in aerodynamic behaviour. The shape 4 can be recommended in engineering practice because its characteristic flutter velocities were the highest, which makes the phenomena less possible to happen. On the contrary, the shape 2 should be avoided. The shape 1 can also be proposed as a good solution for systems with $f_2/f_1 > 1.15$ but should not be used at $f_2/f_1 < 1.15$ due to its tendency to sudden jumps. The characteristic feature of the shape 3 is the smallest change in the velocities for different values of f_2/f_1.

The diagrams of the dominant flutter frequency presented in Fig. 15 and 16 confirm the existence of the 2 different regions at the f_2/f_1 space for aerodynamic behaviour of the aeroelastic system.
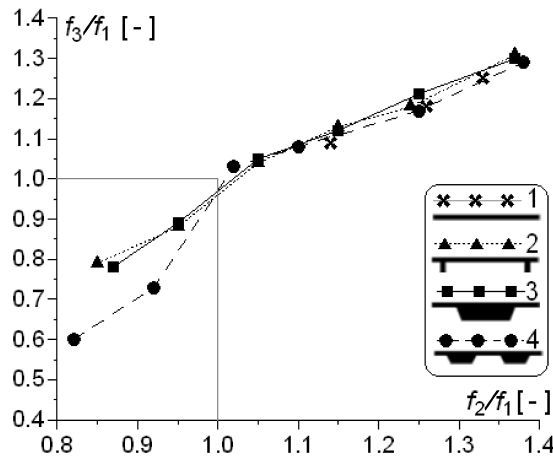

FIG. 15. Dominant flutter frequency for the system without the C dampers.
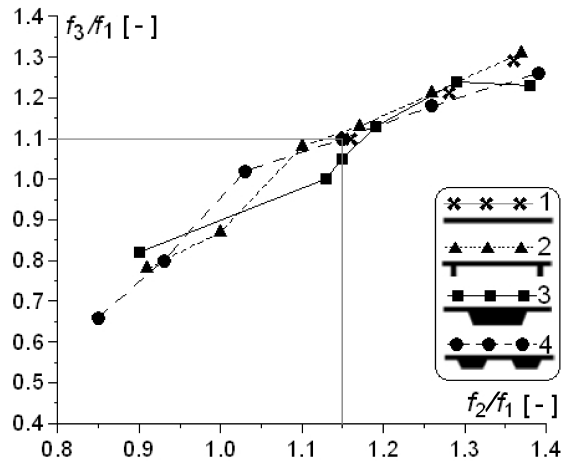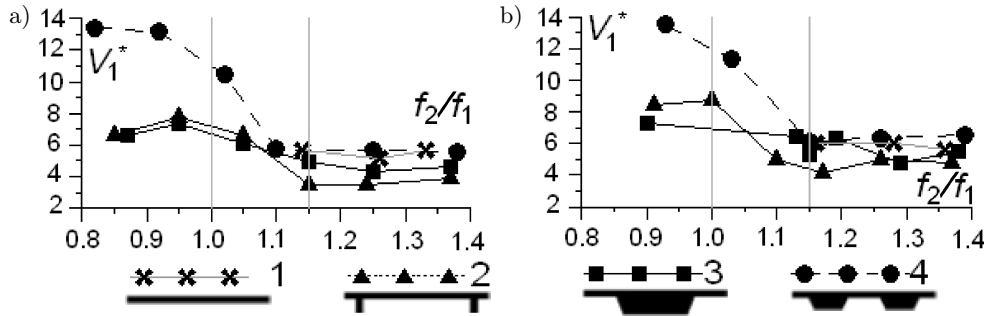
FIG. 16. Dominant flutter frequency for the system with the C dampers.

Again one can notice that for $f_2/f_1 > 1.15$, the influence of the shape decreases in comparison with lower values of the parameter. Here, finally, we can observe an effect directly connected with the system damping. For lower values of damping characteristics, the lost in shape influence on the dominant flutter frequency started at $f_2/f_1 \approx 1.0$ and continued for higher values. As it has be described above, the interval $1.0 < f_2/f_1 < 1.15$ is a transition region for flutter form. These facts let us propose a hypothesis that damping plays an important role in change of flutter form in the interval.

The influence of cross section–shape applied to characteristic flutter velocities and dominant flutter frequency in a consistent way. Creating dimensionless velocities by relating them to the dominant flutter frequency (6.2) one can notice intensification of the effect (see Fig. 17 to 19)

$$(6.2) \qquad V_i^* = \frac{V_i}{f_3 B}, \qquad i = 1, 2, 3.$$

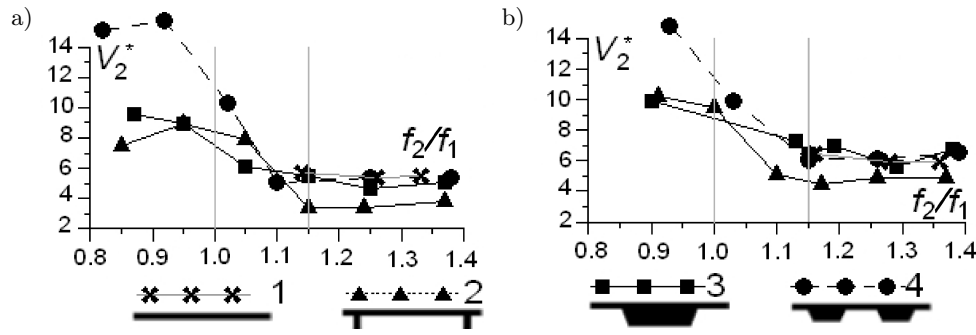FIG. 17. V_1^* [–] a) system without the C dampers b) with the dampers.

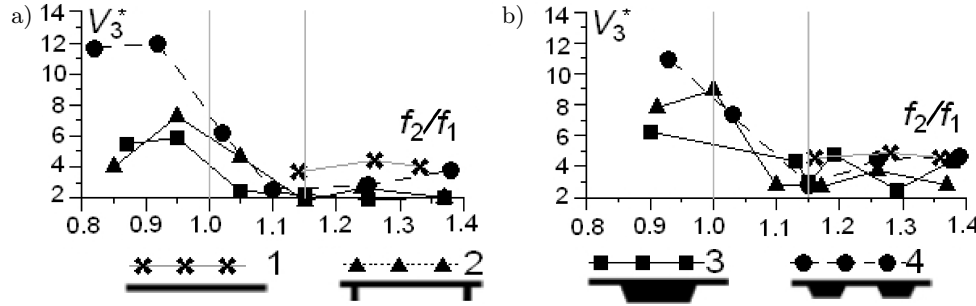FIG. 18. V_2^* [–] a) system without the C dampers b) with the dampers.

FIG. 19. V_3^* [–] a) system without the C dampers b) with the dampers.

The first dimensionless velocity V_1^* is the reciprocal of the Strouhal number previously given in the Tables 4–7. The values (i.e. St $= 1/V_1^*$) are presented in Fig. 20.
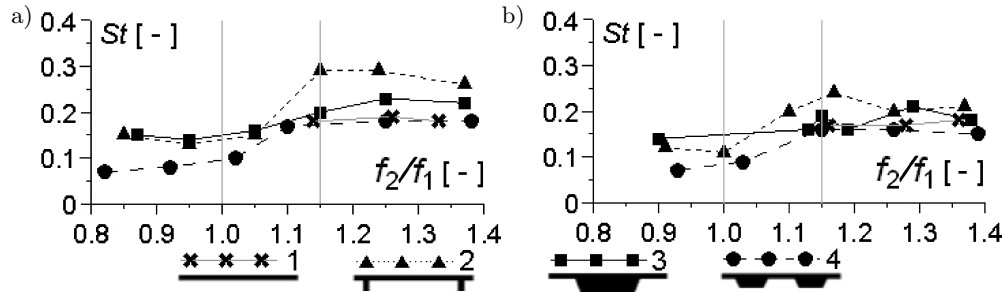

FIG. 20. St $= 1/V_1^*$ [–] a) system without the C dampers b) with the dampers.

Taking into consideration the order of Strouhal number for vortex-induced vibrations [1], dimensions of the cross-section shape of the model and values of

normal frequencies, it can be estimated that the range of velocity specific to vortex-induced vibration is 1–3 m/s. The experiment showed that critical flutter velocities are significantly higher.

7. Verification

Study of the influence of cross-section shape on the phenomenon of flutter can be found in [9], albeit the authors undertook a different approach. A rectangular cross-section shape with different side ratio but at fixed characteristics of suspension ($f_1/f_2 = 6.0/4.5$ Hz $= 1.33$ and structural damping close to zero) was scrutinized. A rectangular shape with side ratio $B/D = 200/10$ was classified as prone to *torsional branch coupled flutter*. The statement has been confirmed in this paper (see Table 4). The flutter dominant frequency and the velocities under interest are not given in [9] but can be obtained from theoretical solution developed by Theodersen for a flat airfoil based on potential flow and the Kutta condition [10]. Table 8 compares the obtained experimental results with theoretical ones.

Table 8. Obtained experimental values (Table 4) against theoretical solution for cross-section 1.

f_2/f_1 [–]		1.14	1.26	1.33
V_1 [m/s]	experimental	7.40	7.24	8.39
	theoretical	7.07	9.22	11.24
f_3 [Hz]	experimental	3.24	3.50	3.69
	theoretical	3.21	3.43	3.65

It can be seen from the Table 8 that the obtained experimental output agrees with the theoretical estimations at acceptable level.

8. Application

Table 9 gives modal characteristics of real structures: 2 footbridges and 2 bridges [11]. The results come from computer FEA simulations and have been confirmed in situ. All of them are typical structures build in Poland in recent years. As we can see, the suspension parameter f_2/f_1, i.e. the ratio of rotational to vertical vibrations frequency, is usually larger than 1.15, which means that the structures fall into the region where cross-section shape plays less important role in the aerodynamic response. It means that the form of flutter, if it happens, should be rotational with domination of the leeward edge.

Table 9. Modal characteristics of selected structures [11].

Structure, span [m]	f_1 [Hz]	f_2 [Hz]	f_2/f_1 [–]
Footbridge in Piwniczna, 102	0.59	0.68	1.15
Footbridge in Tylmanowa, 80	1.47	2.14	1.46
Siekierkowski Bridge in Warsaw, 250	0.43	0.49	1.14
John Paul II Bridge in Gdańsk, 230	0.41	0.66	1.61

9. Conclusions

1. There was a success in inducing the phenomenon of flutter in a laboratory for different cross-section shapes and at different characteristics of suspension.

2. The ratio of rotational to vertical oscillations frequency was chosen as a parameter describing the suspension.

3. Transition in flutter form and lost in significance of the cross-section shape on the phenomenon was observed while changing the above parameter from 0.8 to 1.4.

4. Typical footbridges and bridges fall into a category of structures for which the cross-section shape does not play the most important role in the flutter phenomenon.

5. It seams that the cross-section shape, together with damping, plays an important role within the transition region for flutter form.

6. Further investigations are needed to confirm the observations.

Acknowledgments

References

1. A. FLAGA, *Wind engineering fundamentals and applications* [in Polish], ARKADY, Warszawa 2008.

2. T. MIYATA, *Historical view of long–span bridge aerodynamics*, J. Wind Eng. and Ind. Aerodyn., **91**, 1393–1410, 2003.

3. M. GO, R. ZHANG, H. XIANG, *Identification of flutter derivatives of bridge decks*, J. Wind Eng. and Ind. Aerodyn., **84**, 151–162, 2000.

4. A.G. CHOWDHURY, P.P. SARKAR, *A new technique for identification of eighteen flutter derivatives using a three-degrees-of-freedom section model*, Eng. Structures **25**, 1763–1772, 2003.

5. G. Bartoli, C. Mannini, *A simplified approach to bridge deck flutter*, J. Wind Eng. and Ind. Aerodyn., **96**, 229–256, 2008.

6. A. Larsen, J.H. Walther, *Aeroelastic analysis of bridge girder sections based on discrete vortex simulations*, J. Wind Eng. and Ind. Aerodyn., **67–68**, 253–265, 1997.

7. A. Larsen, J.H. Walther, *Discrete vortex simulation of flow around five generic bridge deck sections*, J. Wind Eng. and Ind. Aerodyn., **77–78**, 591–602, 1998.

8. I. Taylor, M. Vezza, *Calculation of the flow field around a square section cylinder undergoing forced transverse oscillations using a discrete vortex method*, J. Wind Eng. and Ind. Aerodyn., **82**, 271–291, 1999.

9. M. Matsumoto, Y. Taniwaki, R. Shijo, *Frequency characteristics in various flutter instabilities of bridge girders*, J. Wind Eng. and Ind. Aerodyn., **90**, 1973–1980, 2002.

10. T. Theodorsen, *General theory of aerodynamic instability and the mechanism of flutter*, NASA NTRS, NACA–TR–**496**, 1979.

11. A. Flaga, E. Błazik–Borowa, J. Podgórski, *Aerodynamics of slender buildings and cable-rod structures* [in Polish], Wydawnictwo Politechniki Lubelskiej, Lublin 2004.